Protein Science (1993), *2*, 1106–1113. Cambridge University Press. Printed in the USA.

Crystal structure to 2.45 Å resolution of a monoclonal Fab specific for the *Brucella* A cell wall polysaccharide antigen

D.R. ROSE,[1] M. PRZYBYLSKA,[2] R.J. TO,[2] C.S. KAYDEN,[2] R.P. OOMEN,[3] E. VORBERG,[2] N.M. YOUNG,[2] AND D.R. BUNDLE[2]

[1] Ontario Cancer Institute and Department of Medical Biophysics, University of Toronto, 500 Sherbourne Street, Toronto, Ontario M4X 1K9, Canada
[2] Institute for Biological Sciences, National Research Council Canada, Ottawa, Ontario K1A 0R6, Canada
[3] Connaught Laboratories, 1755 Steeles Avenue West, Willowdale, Ontario M2R 3T4, Canada

(RECEIVED January 22, 1993; REVISED MANUSCRIPT RECEIVED March 24, 1993)

Abstract

The atomic structure of an antibody antigen-binding fragment (Fab) at 2.45 Å resolution shows that polysaccharide antigen conformation and Fab structure dictated by combinatorial diversity and domain association are responsible for the fine specificity of the *Brucella*-specific antibody, YsT9.1. It discriminates the *Brucella abortus* A antigen from the nearly identical *Brucella melitensis* M antigen by forming a groove-type binding site, lined with tyrosine residues, that accommodates the rodlike A antigen but excludes the kinked structure of the M antigen, as envisioned by a model of the antigen built into the combining site. The variable-heavy (V_H) and variable-light (V_L) domains are derived from genes closely related to two used in previously solved structures, M603 and R19.9, respectively. These genes combine in YsT9.1 to form an antibody of totally different specificity. Comparison of this X-ray structure with a previously built model of the YsT9.1 combining site based on these homologies highlights the importance of V_L:V_H association as a determinant of specificity and suggests that small changes at the V_L:V_H interface, unanticipated in modeling, may cause significant modulation of binding-site properties.

Keywords: antibody; carbohydrate; cell-surface antigen; crystallography; Fab

Oligosaccharide epitopes expressed on the surface of bacterial and mammalian cells play important roles in the immune response to disease (Lindberg et al., 1983; Hakomori, 1984), and the investigation of their interactions with antibody-binding sites has important implications for engineering combining sites to these epitopes. The interactions of carbohydrates with antibodies are expected to encompass much smaller interaction surfaces than those seen with globular protein antigens (Amit et al., 1985; Colman et al., 1985; Sheriff et al., 1987). Some years ago, Kabat predicted that two types of anti-carbohydrate sites would occur, described as pockets and grooves (Cisar et al., 1975). To date, only one carbohydrate antigen–Fab complex has been reported at atomic resolution (Cygler et al., 1991), and in that example a small, branched trisaccharide filled the binding site. It therefore represents a pocket type of site. This report describes, in contrast, a groove-shaped site, which is significant because it appears to be appropriate for a larger oligosaccharide with five to six pyranose residues.

The immune response of mice to the gram-negative bacteria, *Brucella abortus* and *Brucella melitensis*, is characterized by a strong secondary response to the cell wall A or M polysaccharide antigens. A family of hybridoma antibodies with high specificities for these antigens has been produced (Bundle et al., 1984, 1989) The two polysaccharides are both homopolymers of the monosaccharide, 4,6-dideoxy-4-formamido-α-D-mannopyranose (common name, perosamine); the A antigen is an α1,2-linked polymer (Fig. 1), whereas the M antigen has a linear pentasaccharide repeating unit of four α1,2- and one α1,3-linked residues (Peters et al., 1990). Analyses of the binding of two members of this family of monoclonal

Reprint requests to: David R. Rose, Ontario Cancer Institute and Department of Medical Biophysics, University of Toronto, 500 Sherbourne Street, Toronto, Ontario M4X 1K9, Canada.

Abbreviations: C, constant; CDR, complementarity determining region; Fab, antigen-binding fragment; F_{obs} and F_{calc}, observed and calculated X-ray scattering factor amplitudes; H, heavy; L, light; PEG, poly(ethylene glycol); V_m, unit-cell volume-to-mass ratio; V, variable.

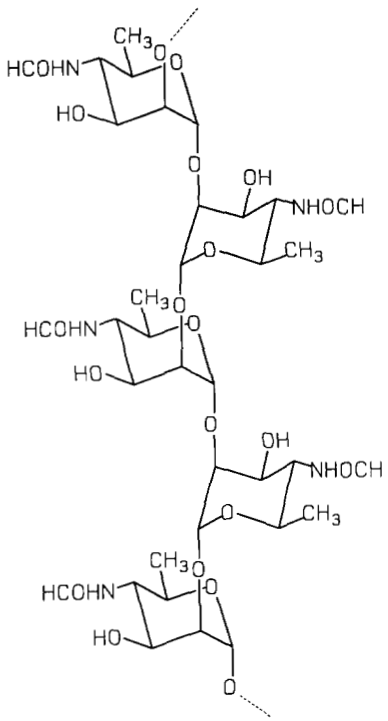

Fig. 1. Chemical structure of the *Brucella* A homopolymer.

antibodies, YsT9.1 (IgG2b,κ) and YsT9.2 (IgG3,κ), by competitive inhibition assays (Bundle et al., 1989; Meikle et al., 1989) identified optimal epitope sizes and led to speculation about the shape and extent of the combining sites (Bundle, 1989).

The antibody YsT9.1, the structure of which is reported here, has the ability to distinguish the A from the M antigen, and the binding site appears to be optimally filled by a pentamer or hexamer sequence of the α1,2-linked A polysaccharide. Thus, it is expected to have a long groove in which the antigen is bound, as envisioned by Kabat and coworkers for nonterminal antigens (Cisar et al., 1975). The antigen conformation has been modeled by potential energy calculations in conjunction with high-resolution NMR studies (Peters et al., 1990) and inferred to approximate a rodlike structure from which formamido and C-5 methyl functions protrude. Consistent with this interpretation, the formamido groups are observed to make a significant contribution to the specificity of the interaction with the binding site (Bundle, 1989). The results reported here constitute the first step in examining this interaction in atomic detail.

Results and discussion

All six CDRs have been positioned with high certainty; a portion of the electron density map around CDR H3 is shown in Figure 2. Two loops in the H-chain constant region, residues H135–H138(129–132)[1] and H161–H168 (155–162), are not clear in the electron density. Although uncertain in detail, the H161–168(155–162) loop probably obstructs access to the antigen-binding site. All four chain termini are clear. No water molecules were included in the refinement. A total of 29 possible locations for bound water were found, none of which are in the vicinity of the binding site. As mentioned above, the site is at a region of crystal contacts.

The stereochemistry of the structure was analyzed with the PROCHECK suite of programs of Thornton and colleagues (Morris et al., 1992). Both side-chain and main-chain parameters are consistent with those of other structures at this resolution. No nonglycine residues lie in disallowed regions of the Ramachandran plot; 84% lie in the most favored regions and a further 13% in the additional allowed regions.

The framework region of the Fab YsT9.1 has the usual immunoglobulin fold observed in other Fab crystal structures (see Kinemage 1). The elbow angle between the V_L:V_H and C_L:C_H1 pseudo-twofold axes is 145°. The conformations of the CDR loops were evaluated in terms of the canonical types defined by Chothia et al. (1989). Loops L2, L3, and H1 fall into type 1, L1 into type 2, and H2 into type 4. With the exception of H2, shared by only two other structures (M603 and 4FAB), the individual loop conformations are fairly common.

The antigen-combining site formed by the six CDRs is a deep crevice running some 20 Å, the breadth of the V-domain, approximately perpendicular to the V_L:V_H pseudo-twofold axis (Fig. 3; Kinemage 1). The crevice is narrowed at both ends by the CDRs H3 and L3. The significance of the H3 loop, in particular, will be discussed below. The crevice is about 10 Å deep by 15 Å wide and lined with aromatic side chains. Five tyrosines line the crevice, L32, L49, and L50 along one side, and H32 and H33, as well as Phe H50 along the other side. Tyr H103(97), Trp H47, and Pro H102(98) form the base of the crevice. Slightly offset from the center of the crevice, there is a depression bounded by residues from all three V_L CDRs (Tyr L32, Tyr L50, and Gly L91), as well as Tyr H103(97) of the H3 loop. The side chain of Asn L34, one of the few polar groups in the binding site, forms the bottom of the depression (Kinemage 1).

The YsT9.1 antibody clearly belongs to the groove class of anti-carbohydrate antibody (Cisar et al., 1975). The myeloma antibody, J539, can also be considered a member of this class, but the shapes of the two polysaccharide antigens and, hence, the forms of the grooves, are quite

[1] In the coordinate file submitted to the Brookhaven Protein Data Bank, and thus in the text, the heavy chain is numbered consecutively from H1 to H217 and the light chain from L1 to L214. The L-chain numbering and the H chain to residue 52 correspond to the Kabat system. To aid in interpretation, the H-chain number of the Kabat system is given in parentheses when it differs from the consecutive number quoted in the text.

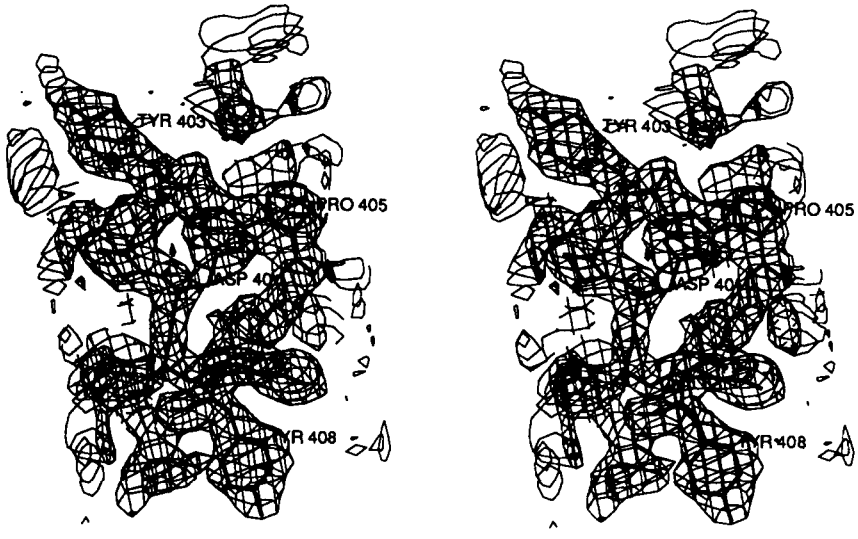

Fig. 2. Stereo electron-density representation of $2F_{obs} - F_{calc}$ map, contoured at 1.0σ, of the third H-chain CDR with the model superimposed. Residue numbers are incremented by 300 such that the label 401 refers to residue H101 (95, Kabat). Image produced with program Chain (Spurlino, pers. comm.).

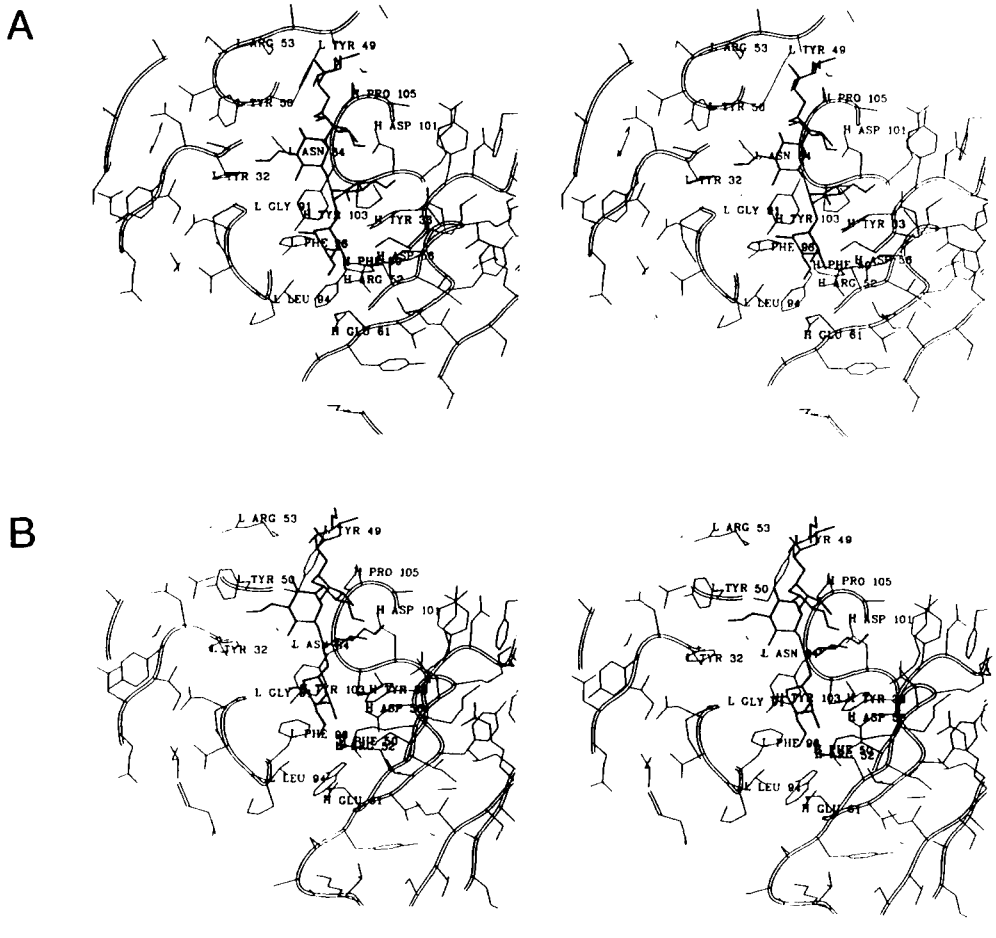

Fig. 3. Two stereo views of the binding crevice with a model of the pentasaccharide hapten, as positioned visually, superimposed. All the side chains are shown as sticks on a smoothed backbone ribbon. The pentasaccharide is in thick lines. Labeled residues are referred to in the text. In both views, the L chain is on the left and the H chain on the right. **A:** View approximately along the V_L:V_H pseudo-twofold axis. This view is approximately reproduced in Kinemage 1. **B:** Rotated from A by about 45° about the horizontal axis. Images produced with the program Setor (Evans, 1993).

different. The *Brucella* A antigen forms a wide helix due to the stacking of the hexose rings that results from the α1,2-linkages. In contrast, the putative ligand for J539 is a β1,6-galactopyranose structure, which has a more elongated form and thus fits a narrower, curved groove in the binding site (Suh et al., 1986).

In order to envision the interactions that the binding site might make with the antigen, a minimum energy model of the pentamer was superimposed visually onto the site, assuming no major conformational change on association. This is not intended to be a docking calculation nor a definitive proposal of the mode of binding, but a study of the dimensions and potential contact atoms of the crevice and the polysaccharide. The modeling identified several side chains that might play roles in binding. These are described here and illustrated in Figure 3 and in Kinemage 2. In its most ordered minimum-energy conformation, the *Brucella* A antigen adopts a rodlike structure of cross section about 11 Å, with the sugars making up the core of the rod, formed by the ethylene glycol-like atom string O1-C2-C1-O2′ (Figs. 1, 3) that defines the α1,2-linkage (Peters et al., 1990). The 6-deoxy and 4-formamido groups are the most exposed features of this three-dimensional structure (Fig. 3; Kinemage 2) with a distance of 17.3 Å separating the first and fifth formamido groups. Two charged side chains, Arg H52 and L53, spaced 21 Å apart at opposite ends of the cleft are disposed to potentially interact with these groups via strong hydrogen bonds (Quiocho, 1989). The hydrophobic depression described above, specifically, Tyr L32 and Tyr L50, is well located to associate with hydrophobic regions in the middle of the pentasaccharide, though Asn L34 is unlikely to be in direct contact with the antigen. Asp H101(95), however, protrudes into the binding region and might well form a hydrogen bond to the formamido substituent of a sugar. Pro H105(99) and Tyr H103(97) would then interact with portions of that and the subsequent sugar rings. With one end of the pentasaccharide positioned by residues Arg H52, Asp H56(53), and Leu L94, the other end would extend to the vicinity of Arg L53 and Tyr L50. The groove itself extends further such that a sixth sugar might contact Tyr L49. These observations are therefore consistent with the expected dimensions of an antigenic determinant of five to six α1,2-linked saccharides. This would also suggest how the antibody discriminates the closely related *Brucella* M antigen, where the presence of an α1,3-linkage every fifth residue introduces a serious kink into the rodlike A antigen.

Comparison with homology-modeled structure

Several combining site features predicted from the modeling study of the YsT9.1 combining site (Oomen et al., 1991) were confirmed by the crystal structure. The overall shape of the combining site, a groove running parallel to the V_L:V_H interface, was predicted correctly, as was the depression near the center of the Fv domain, postulated to be an important antigen-recognition subsite. In the crystal structure, this depression is displaced somewhat toward the V_L side. The importance of the CDR tyrosine residues in defining the topology of the combining site was confirmed. Many, but not all, the side chains were modeled in the correct rotameric forms.

The main inaccuracies in the modeling result from the template structures used as the starting basis. Specifically, aspects that could not be modeled correctly were the structure of the H3 loop and the V_L:V_H association. These aspects are interdependent, as residues at the C-terminal end of the H3 CDR form part of the V_L:V_H interface. The positioning of V_L relative to V_H was modeled after M603, in accord with previous studies that stressed the conservation of residues and geometrical invariance in the packing of variable regions (Novotny & Haber, 1985; Chothia & Lesk, 1987). Although the angle relating V_L and V_H was accurately predicted, in order to effect a reasonable superposition of the model on the crystal structure, a translational component of about 3 Å had to be introduced as well.

The difficulty in predicting the association of V_L and V_H is clearly one that needs to be addressed in the context of modeling an entire combining site. A complication is the role of the noncanonical H3 loop in determining the association. The H3 loop of YsT9.1 is unusually rich in residues with unique conformational properties (e.g., Pro, Gly). As a result, the extension of the H3 loop into the central V domain β-barrel was not predicted accurately, implying that there are mutual adjustments of side chains or shifting of secondary structural elements as a result of differing V_L:V_H association. This phenomenon is exemplified in the recent report of the structure of the anti-peptide Fab 17/9 (Rini et al., 1992). In retrospect, the V_L:V_H association in the YsT9.1 crystal structure differs from the currently available atomic structures. Thus, it could not have been predicted beforehand using a strict homology-based modeling approach.

Recurrence of similar gene segments in different structural contexts

Homologies found from the amino acid and gene sequences of the H- and L-chain variable regions (Bundle et al., in prep.) have shown that these sequences are very similar to V region sequences of other known Fab structures. The YsT9.1 H chain appears to be encoded by the T15-V11 V_H germline gene, which is closely related to that used by many phosphocholine-binding murine antibodies (T15-V1; Crews et al., 1981) including M603, the crystal structure of which is known (Satow et al., 1987). There are 18 sequence differences in the first 100 residues of the H chains of YsT9.1 and M603. Seven of these differences occur in CDRs 1 and 2, and there are no insertions and deletions (Fig. 1 of Oomen et al. [1991]). In

addition, the L-chain variable gene of YsT9.1 appears to be derived from the Vκ10-Ars-A gene (Meek et al., 1987). This segment is also used by two anti-phenylarsonate monoclonal Fabs of which crystal structures have been reported, R19.9 (Lascombe et al., 1989) and 36-71 (Strong et al., 1990). Two structurally important changes in YsT9.1 are Tyr for Ser (L30) and Ile for Phe (L87). Fab 36-71 has Asn at position L30 and differs from the germline at eight others. The joining (J) segments are also closely related. In YsT9.1, there are two changes from the germline Jκ1, Phe for Arg (L96) and Ser for Gly (L100), whereas 36-71 has only an Ala substitution for Thr at the V-J junction (position L93).

In order to assess the structural significance of these changes, the V_H region of M603 and the V_L region of 36-71 were superimposed individually on the corresponding parts of YsT9.1. Figure 4 and Kinemage 3 show the superposition of the composite model onto YsT9.1. The positions of the L-chain CDR residues are essentially unchanged. The L3 loop does show a slight repositioning away from the center of the binding site in YsT9.1 as compared to 36-71, consistent with the formation of a groove rather than a pocket-shaped site. In the H-chain comparison, the third CDR loop, which is not encoded in the shared genes, shows major differences in the comparison, emphasizing its importance in generating the shape of the binding site. Specifically, M603 has a longer H3 loop than YsT9.1 by about five residues. This loop in M603 extends into the area occupied by the binding crevice of YsT9.1. The H1 and H2 loops show smaller but still significant differences between the two structures. Especially noticeable are side-chain replacements at the tips of the loops, H30–32 and H55–57. Thus, in this analysis, the third CDRs are crucial to the overall topology of each binding region. However, modest movements in other loops can have significant effects on the shape.

This simple comparison does not address the issue of how the overall combining site is constructed by the association of the V_L region (in M603) and the V_H region (in 36-71) with the portions in common to YsT9.1. Domain association clearly plays a role in maintaining specificity and affinity (Bhat et al., 1990). Nevertheless, this analysis provides a view at the atomic level of how regions of common local three-dimensional structure can form, in the context of different partner regions, combining sites with completely different properties.

Fig. 4. Superposition of YsT9.1 on R19.9/M603 composite model (smoothed main chain) in stereo. The composite model is shown in thin lines; YsT9.1 in thick lines. **A:** Approximately perpendicular to the V_L:V_H pseudo-twofold axis. **B:** Approximately parallel to the axis. Image made with program InsightII (Biosym Technologies, Inc.).

Materials and methods

Fab preparation and crystallization

Hybridoma antibodies were raised in mice as previously described (Bundle et al., 1984). Protein A-purified YsT9.1 (24 mg) dialyzed into 50 mM Tris buffer, pH 8.05, containing 150 mM sodium chloride, 0.05 mM dithiothreitol, and 2 mM EDTA, was digested with papain freshly prepared from mercuripapain, with an enzyme–substrate ratio of 1:200, for 22 h at 37 °C. The digest was dialyzed against 10 mM Tris containing 10 mM sodium chloride, pH 8.0. This solution, diluted with 80 mL of 10 mM Tris buffer was applied to a DEAE-cellulose column (Whatman DE-52 column 0.7 × 10.0 cm) equilibrated with 10 mM Tris buffer. After washing with 10 mL of the same buffer, a sodium chloride gradient 0–100 mM in 400 mL volume was applied to the column. Three distinct peaks eluted at 4 mM, 10 mM, and 15 mM sodium chloride with yields of 3.2, 4, and 2.2 mg of Fab, respectively. Each peak gave a single band on isoelectric focussing gels. For crystallization, peak II was concentrated to 7.5 mg/mL and dialyzed against 10 mM Tris buffer, pH 8.0, with 3 mM sodium azide in a Schleicher and Schuell apparatus. Collodion membranes with an average retention of 10 kDa were used.

Seed crystals were obtained in hanging droplets consisting of 4 μL of Fab solution, 1 μL of 0.12 M ammonium sulfate, 0.8 μL of 0.5 M Tris buffer, pH 7.2, and 4.2 μL of 20% (w/v) PEG of average molecular weight 8,000, recrystallized (Weininger & Banaszak, 1978). The reservoir contained 1 mL of 34% PEG 8000 with a trace of sodium azide. To obtain larger crystals, droplets as described above were equilibrated over reservoirs of 23% PEG 8000 for 16 h, and seeds washed in 20% PEG were then introduced. In order to maximize the size of the crystals and to prevent their deterioration on standing, a double cell (Przybylska, 1989) was used to increase the PEG concentration of the reservoir to 28%.

The unit cell of the monoclinic crystal is space group $P2_1$, $a = 73.35$ Å, $b = 133.08$ Å, $c = 46.82$ Å, $\beta = 95.03°$. There are two Fabs in the asymmetric unit with a V_m ratio (Matthews, 1968) of 2.28 Å^3/Da. In the same conditions but at a higher pH (8.0), orthorhombic crystals grew, in space group $P2_12_12_1$ with $a = 75.73$ Å, $b = 126.82$ Å, $c = 46.82$ Å, and a V_m of 2.25 Å^3/Da, with only one Fab per asymmetric unit. Despite the different space groups, the unit cell sizes are very similar, indicating that the Fabs may be similarly arranged in the two crystals. The orthorhombic form was chosen for the study reported here because of the single Fab in the asymmetric unit.

Data collection

X-ray diffraction data from a single crystal were measured on a San Diego Multiwire System two-detector setup mounted on a Rigaku RU-200 rotating anode X-ray generator operated at 40 kV, 150 mA. With the detectors positioned at θ values of −9.8° and 25.0°, seven data collection sweeps were used to sample the diffraction sphere. A total of 37,288 measurements were made of 15,355 unique data (of a possible 17,763) at 2.42 Å resolution with an Rsym[2] of 5.17% on intensity. The data set is 94.2% complete to 2.61 Å resolution and the 2.54–2.42-Å range is approximately 60% complete. No explicit corrections for radiation damage or absorption were applied.

Molecular replacement and refinement

Molecular replacement was carried out with the Crowther (1972) cross rotation program and the correlation search program BRUTE (Fujinaga & Read, 1987). Several Fab model coordinates were obtained from the Brookhaven Protein Data Bank (Bernstein et al., 1977) or directly from the authors (HED10; Cygler et al., 1987). In order to facilitate the comparison of results, the models were placed in approximately the same starting orientation. The coordinates for Fab KOL (Matsushima et al., 1978) were oriented in an Eulerian coordinate frame such that the z-axis was coincident with the pseudo-twofold axis relating the C_L and C_H1 units. The C domains of the other models were then superimposed by least-squares onto the KOL C domain. Refinement has been carried out by both least-squares fitting (PROLSQ; Hendrickson & Konnert, 1979) and simulated annealing with molecular dynamics (XPLOR; Brunger, 1988) and rebuilding with the FRODO (Jones, 1978) software.

The rotation function was run independently for the C and V domains of each model. Peaks were identified that were significantly above the noise level and consistent for a number of models and program parameters (number of data, resolution range, Patterson cut-off radii). The clearest results were with the C domain of HED10 and the V domain of J539 (Suh et al., 1986). For example, with data in a resolution range of 8–5 Å and a cut-off radius of 29 Å, the C region gave a rotation solution at a height of 4.3 standard deviations (SD), 0.5 SD above the next unrelated peak, and the V region at a height of 5.1 SD, 0.7 SD above the next peak.

The translation search was straightforward for the intact C domain. With the domain positioned roughly, the two units, C_L and C_H1, were refined in six dimensions (three rotation and three translation) as separate rigid bodies. The results, shown in Table 1, indicate that, although a fairly significant rotational difference was found in the relative position of the two C units compared to their association in HED10, the translational component was very close (within 1.3 Å). The V domain, on the other hand, did not give a clear result in isolation. It was only

[2] Rsym = $\Sigma_j \Sigma_i |I_i - \bar{I}_i| / \Sigma_i \bar{I}_i$, over i observations of average intensity $\bar{I}_i$, for each reflection, j.

Table 1. *Molecular replacement results: Final rotation angles and translation vectors for each of the four domains*[a]

Search region (model)	Rotation angle (°)			Translation component (Å)		
	α	β	γ	x	y	z
C_L (HED10)	163.88	38.47	265.76	4.8	18.9	2.0
C_H1 (HED10)	168.05	39.73	260.42	4.6	18.4	3.3
V_L (J539)	186.29	48.43	250.01	0.1	16.9	3.0
V_H (J539)	181.00	43.04	259.41	1.4	13.8	3.6

[a] Final correlation: 0.4096. Correlation = $\sum \Delta_{obs} * \Delta_{calc} / [(\Delta_{obs} * \Delta_{obs}) * (\Delta_{calc} * \Delta_{calc})]^{1/2}$, over all reflections, where $\Delta_{obs} = |I_{obs} - \langle I_{obs} \rangle|$ and $\langle I_{obs} \rangle$ = average I_{obs}, and similarly for Δ_{calc}.

when the C domain was present in its correct position that a successful V result was obtained. Table 1 indicates that although the angular differences in the V_H and V_L association from the starting model are somewhat higher, they are still comparable to those for the C domain. However, the translational component compared to the model, over 3 Å in the y direction in particular, is strikingly different. In this instance, it seems that the relative translational difference in the association between units is at least as important as the rotational difference in obtaining strong molecular replacement solutions.

Once the models had been positioned, the amino acid sequence was changed to that determined for YsT9.1 (Bundle et al., in prep.). As the refinement progressed the antigen-binding loops, which had been removed previously, were rebuilt into electron density maps calculated with coefficients $2mF_{obs} - DF_{calc}$ derived from the SIGMAA program of Read (1986). The current refinement statistics are presented in Table 2. The present model consists of 214 L-chain residues and 217 H-chain residues.

Coordinates of the current model and structure factor observations reported in this paper have been deposited with the Brookhaven Protein Data Bank (Bernstein et al., 1977) (codes 1MAM and R1MAMSF).

Table 2. *Final refinement statistics: R-factors and deviations from ideality of the model following the final refinement*

	Deviation	Restraint
Root mean square deviations from ideality		
Bond distances (Å)	0.013	0.020
Angles (Å)	0.034	0.030
Planes (Å)	0.012	0.020
Planar torsions (°)	2.2	3.0

Resolution range (Å)	Number of reflections	*R*-factors Shell	*R*-factors Sphere
R-factors (all data >0)[a]			
6.0–4.0	2,815	0.191	0.191
4.0–3.2	3,571	0.195	0.193
3.2–2.8	3,429	0.232	0.203
2.8–2.6	2,518	0.255	0.210
2.6–2.45	1,750	0.270	0.215

Ramachandran plot analysis (non-Gly) from PROCHECK (Morris et al., 1992)	
Residues in most favored regions	311 (83.6%[b])
Residues in additional allowed regions	49 (13.2%)
Residues in generously allowed regions	12 (3.2%)
Residues in disallowed regions	0 (0.0%)

[a] Protein atoms (non-hydrogen) included in refinement: 3,296.
[b] Typical value for 2.5-Å structures: 76.6%.

References

Amit, A.G., Mariuzza, R.A., Phillips, S.E.V., & Poljak, R.J. (1985). Three-dimensional structure of an antigen-antibody complex at 6 Å resolution. *Nature 313*, 156–158.

Bernstein, F.C., Koetzle, T.F., Williams, G.J.B., Meyer, E.F., Jr., Brice, M.D., Rodgers, J.D., Kennard, O., Shimanouchi, T., & Tasoumi, M. (1977). The Protein Data Bank: A computer archival file for macromolecular structures. *J. Mol. Biol. 112*, 535–542.

Bhat, T.N., Bentley, G.A., Fischmann, T.O., Boulot, G., & Poljak, R.J. (1990). Small rearrangements in structures of Fv and Fab fragments of antibody D1.3 on antigen binding. *Nature 347*, 483–485.

Brunger, A.T. (1988). Crystallographic refinement by simulated annealing. *J. Mol. Biol. 203*, 803–816.

Bundle, D.R. (1989). Antibody combining sites and oligosaccharide determinants studied by competitive binding, sequencing and X-ray crystallography. *Pure Appl. Chem. 61*, 1171–1180.

Bundle, D.R., Cherwonogrodzky, J.W., Gidney, M.A.J., Meikle, P.J., Perry, M.B., & Peters, T. (1989). Definition of *Brucella* A and M epitopes by monoclonal typing reagents and synthetic oligosaccharides. *Infect. Immun. 57*, 2829–2836.

Bundle, D.R., Gidney, M.A.J., Perry, M.B., Duncan, J.R., & Cherwonogrodzky, J.W. (1984). Serological confirmation of *Brucella abortus* and *Yersinia enterocolitica* O:9 O-antigens by monoclonal antibodies. *Infect. Immun. 46*, 389–393.

Chothia, C. & Lesk, A. (1987). Canonical structures for the hypervariable regions of immunoglobulins. *J. Mol. Biol. 196*, 901–917.

Chothia, C., Lesk, A.M., Tramontano, A., Levitt, M., Smith-Gill, S.J., Air, G., Sheriff, S., Padlan, E.A., Davies, D., Tulip, W.R., Colman, P.M., Spinelli, S., Alzari, P.M., & Poljak, R.J. (1989). Conformations of immunoglobulin hypervariable regions. *Nature 242*, 877–883.

Cisar, J., Kabat, E.A., Dorner, M.N., & Liao, J. (1975). Binding properties of immunoglobulin combining sites specific for terminal or nonterminal antigenic determinants in dextran. *J. Exp. Med. 142*, 435–459.

Colman, P.M., Tulloch, P.A., Gough, J.H., Varghese, J.N., Laver, W.G., & Webster, R.C. (1985). The structure of an antineuraminidase monoclonal Fab fragment and its interaction with the antigen. In *Immune Recognition of Protein Antigens* (Laver, W.G. & Air, G.M., Eds.), pp. 77–90. Cold Spring Harbor Laboratory, Cold Spring Harbor, New York.

Crews, S., Griffin, J., Huang, H., Calame, K., & Hood, L. (1981). A single V_H gene segment encodes the immune response to phosphocholine: Somatic mutation is correlated with the class of the antibody. *Cell 25*, 59–68.

Crowther, R.A. (1972). The fast rotation function. In *The Molecular Replacement Method* (Rossmann, M.G., Ed.), pp. 173–178. Gordon & Breach, New York.

Cygler, M., Boodhoo, A., Lee, J.S., & Anderson, W.F. (1987). Crystallization and structure determination of an autoimmune anti-

poly(dT) immunoglobulin Fab fragment at 3.0 Å resolution. *J. Biol. Chem. 262*, 643–648.

Cygler, M., Rose, D.R., & Bundle, D.R. (1991). Recognition of a cell-surface oligosaccharide of pathogenic *Salmonella* by an antibody Fab fragment. *Science 253*, 442–445.

Evans, S.V. (1993). SETOR: Hardware lighted three-dimensional solid model representations of macromolecules. *J. Mol. Graphics*, in press.

Fujinaga, M. & Read, R. (1987). Experiences with a new translation function program. *J. Appl. Crystallogr. 20*, 517–521.

Hakomori, S. (1984). Tumour-associated carbohydrate antigens. *Annu. Rev. Immunol. 2*, 103–126.

Hendrickson, W.A. & Konnert, J.H. (1979). Stereochemically restrained crystallographic least-squares refinement of macromolecule structures. In *Biomolecular Structure, Conformation, Function & Evolution*, Vol. 1 (Srinivasan, R., Ed.), pp. 43–57. Pergamon Press, New York.

Jones, T.A. (1978). A graphics model building and refinement system for macromolecules. *J. Appl. Crystallogr. 11*, 268–272.

Lascombe, M.-B., Alzari, P.M., Boulot, G., Saludjian, P., Tougard, P., Berek, C., Haba, S., Rosen, E.M., Nisonoff, A., & Poljak, R.J. (1989). Three-dimensional structure of Fab R19.9, a monoclonal murine antibody specific for the *p*-azobenzenearsonate group. *Proc. Natl. Acad. Sci. USA 86*, 607–611.

Lindberg, A.A., Wollin, R., Bruse, G., Ekwall, E., & Svenson, S. (1983). Immunology and immunochemistry of synthetic and semi-synthetic *Salmonella* O-antigen-specific glycoconjugates. *Am. Chem. Soc. Symp. Ser. 231*, 83–118.

Matsushima, M., Marquart, M., Jones, T.A., Colman, P.M., Bartels, K., Huber, R., & Palm, W. (1978). Crystal structure of the human Fab fragment KOL and its comparison with the intact KOL molecule. *J. Mol. Biol. 121*, 441–459.

Matthews, B.W. (1968). Solvent content of protein crystals. *J. Mol. Biol. 33*, 491–497.

Meek, K., Sanz, I., Rathbun, G., Nisonoff, A., & Capra, J.D. (1987). Identity of the Vκ10-Ars-A gene segments of the A/J and BALB/c strains. *Proc. Natl. Acad. Sci. USA 84*, 6244–6248.

Meikle, P.J., Perry, M.B., Cherwonogrodzky, J.W., & Bundle, D.R. (1989). The fine structure of A and M antigens from *Brucella* biovars. *Infect. Immun. 57*, 2820–2828.

Morris, A.L., MacArthur, M.W., Hutchinson, E.G., & Thornton, J.M. (1992). Stereochemical quality of protein structure coordinates. *Proteins Struct. Funct. Genet. 12*, 345–364.

Novotny, J. & Haber, E. (1985). Structural invariants of antigen binding: Comparison of immunoglobulin V_L–V_H and V_L–V_L domain dimers. *Proc. Natl. Acad. Sci. USA 82*, 4592–4596.

Oomen, R., Young, N.M., & Bundle, D.R. (1991). Molecular modelling of antibody–antigen complexes between the *Brucella abortus* O-chain polysaccharide and a specific monoclonal antibody. *Protein Eng. 4*, 427–433.

Peters, T., Brisson, J.-R., & Bundle, D.R. (1990). Conformational analysis of key disaccharide components of *Brucella* A and M antigens. *Can. J. Chem. 68*, 979–988.

Przybylska, M. (1989). A double cell for controlling nucleation and growth of protein crystals. *J. Appl. Crystallogr. 22*, 115–118.

Quiocho, F.A. (1989). Protein–carbohydrate interactions – Basic molecular features. *Pure Appl. Chem. 61*, 1293–1306.

Read, R. (1986). Improved Fourier coefficients for maps using phases from partial structures with errors. *Acta Crystallogr. A 42*, 140–149.

Rini, J.M., Schulze-Gahman, U., & Wilson, I.A. (1992). Structural evidence for induced fit as a mechanism for antibody–antigen recognition. *Science 255*, 959–965.

Satow, Y., Cohen, G.H., Padlan, E.A., & Davies, D.R. (1987). Phosphocholine binding immunoglobulin Fab MC/PC603. An X-ray diffraction study at 2.7 Å. *J. Mol. Biol. 190*, 593–604.

Sheriff, S., Silverton, E.W., Padlan, E.A., Cohen, G.H., Smith-Gill, S.J., Finzel, S.C., & Davies, D.R. (1987). The three-dimensional structure of an antibody–antigen complex. *Proc. Natl. Acad. Sci. USA 84*, 8075–8079.

Strong, R.K., Campbell, R.L., Rose, D.R., Petsko, G.A., Sharon, J., & Margolies, M.N. (1991). The three-dimensional structure of the murine anti-phenylarsonate Fab 36-71 I: X-ray crystallography and modelling of the complex with hapten. *Biochemistry 30*, 3739–3748.

Suh, S.W., Bhat, T.N., Naira, M.A., Cohen, G.H., Rao, D.N., Rudikoff, S., & Davies, D.R. (1986). The galactan-binding immunoglobulin Fab J539: An X-ray diffraction study at 2.6 Å resolution. *Proteins Struct. Funct. Genet. 1*, 75–80.

Weininger, M.S. & Banaszak, L.J. (1978). Mitochondrial malate dehydrogenase. Crystallographic properties of the pig heart enzyme. *J. Mol. Biol. 119*, 443–449.